catalysts

MDPI

Article

Surface Modification of Nanocrystalline TiO_2 Materials with Sulfonated Porphyrins for Visible Light Antimicrobial Therapy

Adam Sułek [1], Barbara Pucelik [1,2], Marcin Kobielusz [1], Przemysław Łabuz [1], Grzegorz Dubin [2] and Janusz M. Dąbrowski [1,*]

1 Faculty of Chemistry, Jagiellonian University, Gronostajowa 2, 30-387 Kraków, Poland; adam-s91@o2.pl (A.S.); barbara.pucelik@uj.edu.pl (B.P.); kobielusz@chemia.uj.edu.pl (M.K.); labuz@chemia.uj.edu.pl (P.Ł.)

2 Malopolska Centre of Biotechnology, Jagiellonian University, Gronostajowa 7A, 30-387 Kraków, Poland; grzegorz.dubin@uj.edu.pl

* Correspondence: jdabrows@chemia.uj.edu.pl; Tel.: +48-12-686-2488; Fax: +48-12-686-2750

Received: 5 September 2019; Accepted: 28 September 2019; Published: 29 September 2019

Abstract: Highly-active, surface-modified anatase TiO_2 nanoparticles were successfully synthesized and characterized. The morphological and optical properties of the obtained (metallo) porphyrin@qTiO_2 materials were evaluated using absorption and fluorescence spectroscopy, scanning electron microscopy (SEM) imaging, and dynamic light scattering (DLS). These hybrid nanoparticles efficiently generated reactive oxygen species (ROS) under blue-light irradiation (420 ± 20 nm) and possessed a unimodal size distribution of 20–70 nm in diameter. The antimicrobial performance of the synthetized agents was examined against Gram-negative and Gram-positive bacteria. After a short-term incubation of microorganisms with nanomaterials (at 1 g/L) and irradiation with blue-light at a dose of 10 J/cm^2, 2–3 logs of *Escherichia coli*, and 3–4 logs of *Staphylococcus aureus* were inactivated. A further decrease in bacteria viability was observed after potentiation photodynamic inactivation (PDI), either by H_2O_2 or KI, resulting in complete microorganism eradication even when using low material concentration (from 0.1 g/L). SEM analysis of bacteria morphology after each mode of PDI suggested different mechanisms of cellular disruption depending on the type of generated oxygen and/or iodide species. These data suggest that TiO_2-based materials modified with sulfonated porphyrins are efficient photocatalysts that could be successfully used in biomedical strategies, most notably, photodynamic inactivation of microorganisms.

Keywords: antimicrobial activity; photocatalysts; TiO_2; nanoparticles; photosensitization; photodynamic inactivation of microorganisms (PDI)

1. Introduction

Application of inorganic semiconductors as heterogeneous photocatalysts, and in particular the role of TiO_2 in environmental and biomedical sciences and technologies, has already been extensively investigated. The most efficient methods in this respect are advanced oxidation processes (AOPs) including environmental [1–4] and biomedical photocatalysis [5–9]. Semiconductor-based photocatalysts are routinely used in the degradation of dyes present in waste-water for the following reasons: (i) they are inexpensive and can be obtained easily in a large-scale preparation; (ii) they are non-toxic; (iii) they exhibit tunable properties that can be modified by the size of the particles, doping, and/or sensitization; (iv) they facilitate electron transfer processes; and (v) they are capable of extending their use without substantial loss in the photocatalytic activity [10]. Furthermore, inorganic

photocatalysts are also known for their photo-antimicrobial properties, being able to inactivate a broad spectrum of pathogenic microorganisms such as bacteria, fungi, and/or viruses [11]. The application of semiconductor nanoparticles as antimicrobial agents seems to be one of the most promising approaches because of the increased antibiotic resistance and lack of effective treatment modality [10].

It is important to note that bacterial diseases are one of the major health problems worldwide [12]. Several factors causing the growth of persistent bacterial infections have been identified, including increased use of antibiotics, immunosuppressive drugs, and surgical procedures [13]. Antimicrobial resistance may be caused by mutation and recombination [10] due to external factors (e.g., radiation or harmful chemicals), as well as by formation of their own matrix, known as biofilm [14]. Photodynamic inactivation (PDI) of microorganisms is a promising alternative method for the treatment of many bacterial diseases [15], including antibiotic-resistant infections [16–18]. The PDI concept is based on an application of a drug—known as a photosensitizer (PS)—that absorbs light and, in the presence of oxygen, generates highly toxic reactive oxygen species (ROS) that oxidize biologically important molecules such as proteins, lipids, and nucleic acids, eventually leading to destruction of pathogens. ROS are generated *via* two major photochemical mechanisms: (i) electron or hydrogen atom transfer with subsequent formation of oxygen-centered radicals (i.e., superoxide ion and hydroxyl radicals), and/or (ii) direct energy transfer from PS in its triplet excited state to O_2, resulting in singlet oxygen ($^1O_2$) production [19,20]. Many studies have shown that $^1O_2$ is highly cytotoxic to bacteria because of its increased permeability through the bacterial membrane [15] and lack of enzyme-based defense system, while other authors demonstrate the bacteria killing as a response to radical stress including $HO^{\bullet}$ formation [21]. Photosensitizers for antimicrobial treatment should have strong visible light absorption and, when activated, lead to the desired biological response [10]. Synthetic *meso*-tetraphenylporphyrin derivatives are particularly versatile starting materials for the design of new photoactive compounds. The introduction of various ionic or nonionic moieties at the peripheral positions of the macrocycle enables modulation of the PS physicochemical properties. In general, cationic porphyrins are more active than anionic or nonionic ones against both Gram-positive and Gram-negative bacteria [22–24]. Recently, we have reported a series of synthetic halogenated tetrapyrrolic derivatives as multifunctional photosensitizers. In subsequent studies, the influence of peripheral substituents in the macrocycle on the photochemical properties and photodynamic efficacy in vitro in both antimicrobial and anticancer approaches has been demonstrated [25]. Nowadays, the development of effective PS for PDI starts from simple metal complexes, through metal-modified macrocycles, up to metal oxides and hybrid (nano)materials [9]. Nanomaterials possess their unique physical and chemical properties as a result of quantum effect, largely influenced by the size and geometry of the material [26,27]. Another beneficial aspect of nanoscale surface topography of the materials is high surface area and its interactions with biologically important molecules present in bacteria cells (e.g., proteins, DNA, or lipid membranes) [28–30]. Nano-sized agents are able to enhance the internalization processes, locally change the microenvironment near the bacteria, increase solubility, and generate ROS responsible for bacterial cells damage [31,32]. Additionally, some metals, such as silver or zinc, are known for their natural antibacterial activity. However, metal oxides must be of sufficient dimensions to avoid agglomeration/aggregation processes that significantly reduce the antimicrobial effect [31]. The properties of bacterial cell walls play a key role in the diffusion of nanoparticles inside the biofilm matrix. Gram-negative bacteria are characterized by a cell wall that contains both an inner cytoplasmic membrane and an outer membrane. Both membranes are separated by the peptidoglycan-containing periplasm. In particular, the outer membrane of Gram-negatives often inhibits the uptake of drugs, antibiotics, and other substances, which makes them more resistant. In contrast, Gram-positive bacteria contain a cytoplasmic membrane with a relatively porous layer of lipoteichoic acids and peptidoglycan that allow the drug to cross. Thus, these species are more prone to photodamage than Gram-negative microorganisms [33]. Moreover, because of the size of the material, optical sensitivity and activity can be changed from the ultraviolet (UV) to the visible region of light [34]. Many applications of TiO_2 in photovoltaics, photocatalysis, and antimicrobial therapy are a result of the optical properties of TiO_2

nanomaterials [35–38]. Unfortunately, titanium dioxide has a relatively wide bandgap and thus can absorb only light at $\lambda < 400$ nm, which may be intrinsically carcinogenic [39]. Various organic dyes can be attached to TiO_2 nanoparticle surfaces *via* functional groups (e.g., –OH, $–SO_3H$, –OOCR) by direct linking between the dyes and the TiO_2 nanoparticle substrate [9,40–43]. Alternative ways of encouraging interaction between the dye and semiconductor are electrostatic interaction through ion exchange, ion-pairing, donor-acceptor interactions, hydrogen bonding, and van der Waals forces. Among the various types of photosensitizers, transition metal complexes with low lying excited states (nitrogen heterocyclics with delocalized π electrons or aromatic ring system) such as (metallo)porphyrins and pthalocyanines [44] capable of the electron injection from their excited states to the conduction band of titania deserve particular attention [45–48]. Synergistic effects from the permeability by nanoparticles and ROS generation by conjugated photosensitizers facilitate photodynamic activity against bacteria, especially under solar irradiation [24,49].

The goal of the present work is to develop visible light-active, nanocrystalline TiO_2-based materials modified by porphyrins in the form of transparent colloidal solutions. All of these materials were comprehensively investigated in terms of their physicochemical characterization and antimicrobial photoactivity against *Escherichia coli* and *Staphylococcus aureus*. The chemical structures of porphyrin derivatives: 5,10,15,20-*tetrakis*-(4-sulfonatophenyl)porphyrin (TPPS); 5,10,15,20-*tetrakis*(2,6-difluoro-3-sulfophenyl)porphyrin (F_2POH), and its metal complexes 5,10,15,20-*tetrakis*(2,6-difluoro-3-sulfophenyl)porphyrin Zn(II) (ZnF_2POH) used in our studies are presented in Scheme 1.

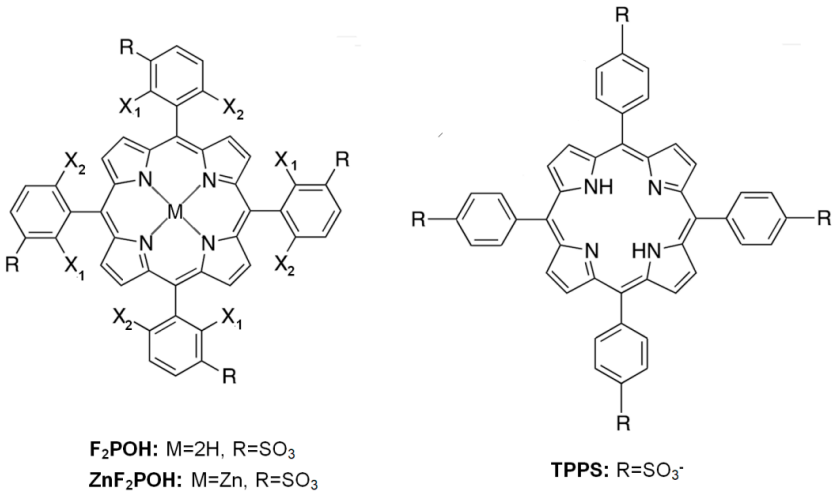

Scheme 1. Chemical structures of porphyrins: free-base halogenated porphyrin (F_2POH, M = 2H) and its Zn-complex (ZnF_2POH, M = Zn), as well as 5,10,15,20-*tetrakis*-(4-sulfonatophenyl)porphyrin (TPPS) used for the modification of $qTiO_2$.

2. Results

2.1. Synthesis, Optical Properties, and Characterization of the Materials

Mixing of the colloidal form of titanium dioxide ($qTiO_2$) with porphyrin solutions in water at slightly acidic pH (pH = 6) resulted in colored colloidal solutions. After addition of $qTiO_2$, the absorption spectrum of F_2POH@$qTiO_2$ was broadened and red-shifted (Figure 1).

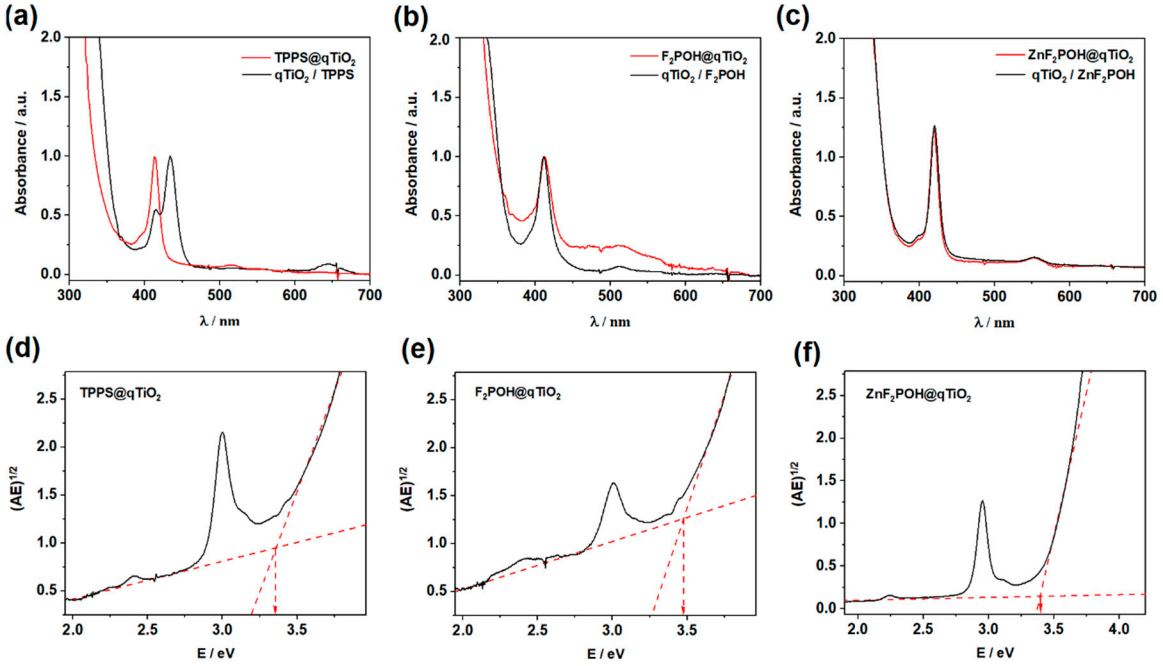

Figure 1. Absorption spectra of $qTiO_2$ overlap with porphyrin (black line) and obtained nanomaterials (red line) after mixing the colloidal solutions of $qTiO_2$ with studied porphyrins: TPPS, 5,10,15,20-*tetrakis*(2,6-difluoro-3-sulfophenyl)porphyrin (F_2POH), 5,10,15,20-*tetrakis*(2,6-difluoro-3-sulfophenyl)porphyrin Zn(II) (ZnF_2POH) (**a**–**c**), and the estimation of the band gaps energy for each material based on the Tauc plot with baseline correction (**d**–**f**).

These changes reflected a suggested electronic interaction between molecules and the support. As illustrated in Figure 1, TPPS attached to $qTiO_2$ showed a blue shift of a Soret band. The spectral changes of TPPS in acidic pH have been previously reported and have been attributed to J-aggregates in which molecules are arranged in head-to-tail (Soret at: 413 nm pH > 7, 433 nm pH < 7) [50]. Thus, the presence of Soret band at 413 nm for TPPS@$qTiO_2$ confirmed this interaction between the semiconductor and non-aggregated PS. The relevant spectral features of studied tetrapyrrolic compounds are reported in Table 1. Other modified porphyrins and their metal complexes have also been successfully used to sensitize TiO_2 [9,51]. On the basis of the Tauc plots (Figure 1d–f; Figure S1) calculated from absorption spectra, the band gap energy for each modified porphyrin@TiO_2 materials were estimated and reached ca. 3.37–3.47 eV. This value was higher than the typical band gap energy for anatase (3.2 eV). Considering the small size of TiO_2 crystals (vide infra), such a large E_g value should be associated with the occurrence of the phenomenon of the quantum size effect (TiO_2 abbreviated as $qTiO_2$) [52,53]. Dynamic light scattering (DLS) was used to characterize the $qTiO_2$ nanomaterials in suspension. The particle size of modified nanomaterials in aqueous solution had a homogeneous distribution with 13, 28, and 68 nm in diameter for TPPS@$qTiO_2$, F_2POH@$qTiO_2$, and ZnF_2POH@$qTiO_2$, respectively (Figure 2). The key parameter of the dispersion stability of nanoparticles is zeta potential (ζ), which is determined by degree of electrostatic repulsion of surface in an ionic environment at the boundary between the Stern layer and the diffuse layer. The obtained values of zeta potentials were in the range from −30 to −20 mV at pH = 6 (Table 1), reflecting a strong binding of all organic modifiers to the titania surface and also a good stability (meant as a lack of aggregation or precipitation in the dark) of colloids.

Table 1. Spectroscopic properties of sulfonyl porphyrin derivatives, mean hydrodynamic diameters, average size of aggregates from scanning electron microscopy (SEM) and zeta potential in water (pH = 6). $qTiO_2$: colloidal form of titanium dioxide, DLS: dynamic light scattering.

	Homogeneous	Heterogeneous (after Modification with $qTiO_2$)				
Sensitizer	**λ_{max}/nm**	**λ_{max}/nm with $qTiO_2$**	**E_g/eV**	**Size/nm DLS**	**Size/nm SEM (Average ± SD)**	**ζ/mV**
TPPS	413, 518, 555, 580, 640	413,516, 556, 645	3.37	13	38 ± 6	−27
F_2POH	410, 509, 541, 575, 640	413, 512, 644	3.47	28	55 ± 11	−26
ZnF_2POH	418, 553	419, 552	3.39	68	41 ± 9	−20
$qTiO_2$			3.50	7	56 ± 24	−33

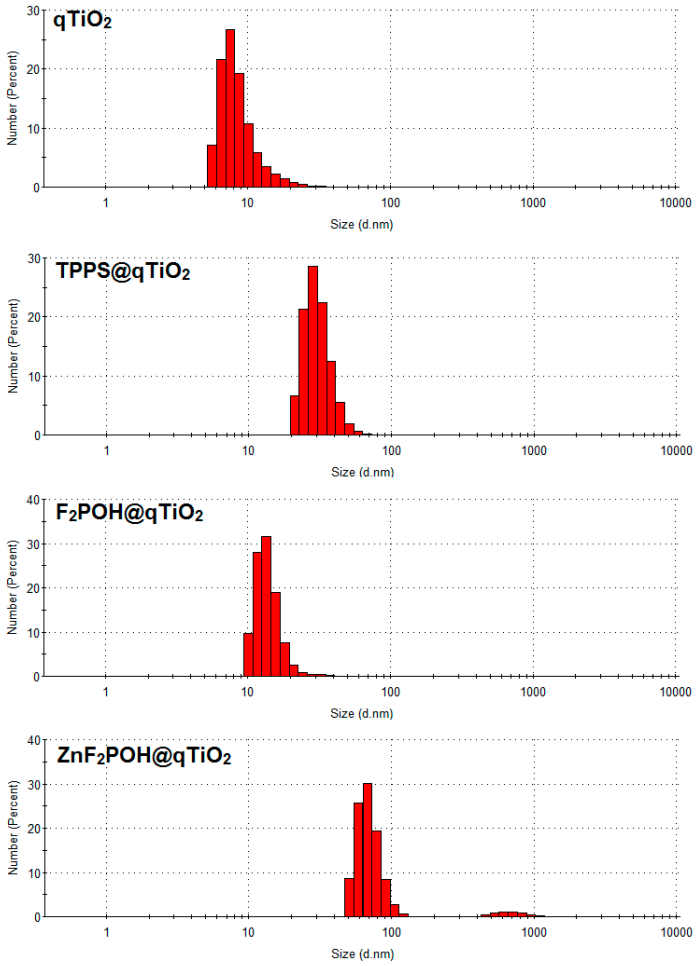

Figure 2. Size distribution of nanocrystalline materials in the aqueous solution.

Scanning Electron Microscopy (SEM) Analysis of Prepared Nanomaterials

The morphological and structural development of the synthesized $qTiO_2$-based nanomaterials was investigated by scanning electron microscopy (SEM). A high magnification SEM image of the nanoparticles shown in Figure 3 indicated that the diameter of the obtained nanomaterials was in the range of 30–50 nm in contrast to unmodified titania, which formed clusters and aggregates with a length of up to 100 nm (Table 1, Figures S2 and S3). SEM analysis clearly demonstrated that after surface modification by porphyrins, the particles did not aggregate. In the field of environmental photocatalysis,

nanoparticles with these particular dimensions generally show higher photocatalytic efficiency due to the large surface-to-volume ratio caused by the reduced particle size. Moreover, nanomaterials of these dimensions may be safely employed in biomedical research and for medicinal purposes.

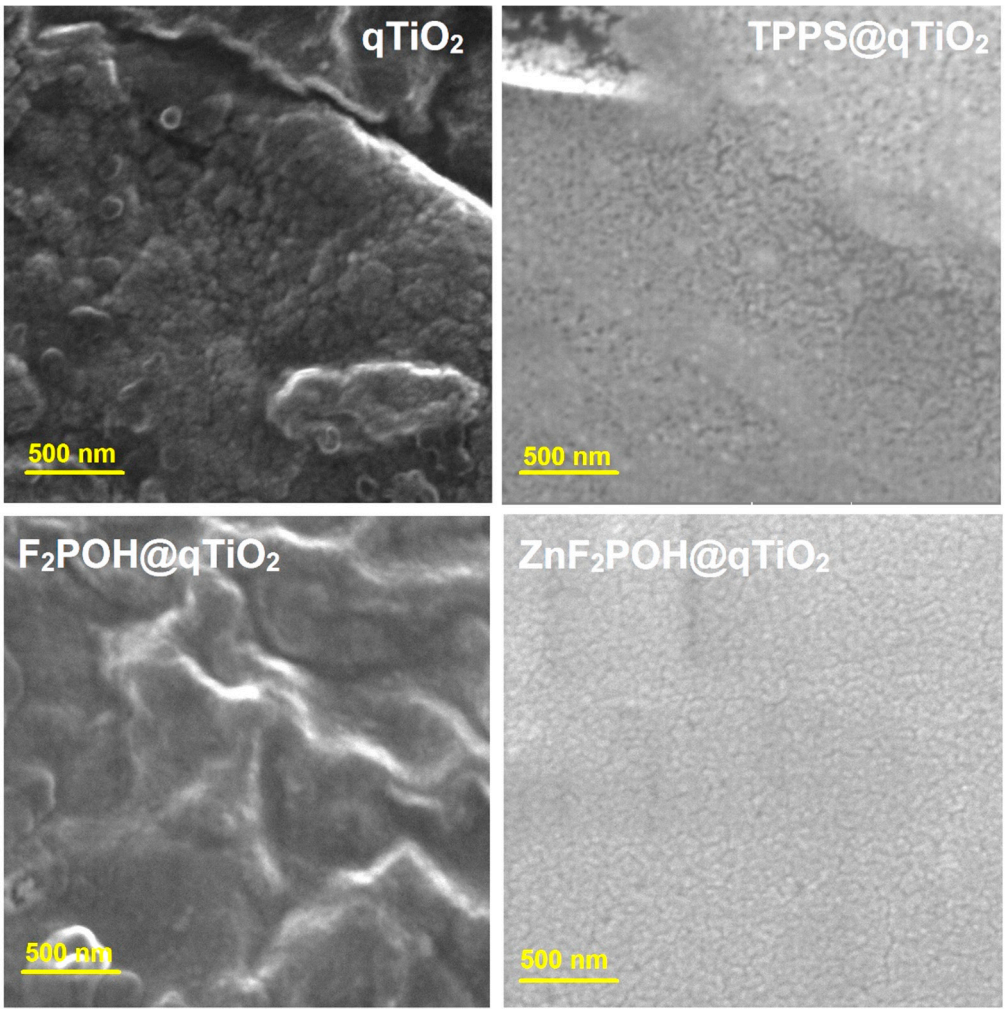

Figure 3. SEM images of nanostructured $qTiO_2$, TPPS@$qTiO_2$, F_2POH@$qTiO_2$, and ZnF_2POH@TiO_2 recorded on carbon tape.

2.2. *Fluorescence Quenching by Colloidal $qTiO_2$ Nanoparticles*

The steady-state fluorescence spectra of sulfonyl porphyrins and their colloidal solution with $qTiO_2$ were recorded in water (pH = 6). The maximum emission wavelengths are listed in Table 2.

Table 2. Photophysical properties of sulfonyl porphyrin derivatives in the absence and presence of colloidal $qTiO_2$ (τ_0 is the lifetime in the absence of colloidal $qTiO_2$, τ_{fl} is the lifetime in the presence of colloidal $qTiO_2$).

Sensitizer	λ_{exp}/nm	Φ_Δ [a]	τ_0	λ_{exp} + $qTiO_2$	τ_{fl} + $qTiO_2$
TPPS	605, 650	0.64	3.41	605 *, 645, 705	5.71
F_2POH	602, 651	0.65	5.04	602 *, 652, 703	7.25
ZnF_2POH	603, 649	0.85	2.28	603, 649	4.38

[a] from reference [9]; * reduced fluorescence emission remained from free porphyrin.

In all the studied scenarios, modification of the $qTiO_2$ surface resulted in a decrease of fluorescence intensity and an increase of fluorescence lifetimes consistently (Figure 4). For materials modified with free base porphyrins, almost complete quenching of the S_1–S_0 emission was observed. Furthermore, the formation of a new emission band derived from the electron transfer from the conduction band (CB) to the ground and oscillation states was observed (Figure 5a,b). The fluorescence intensity of ZnF_2POH was strongly quenched after adsorption at the $qTiO_2$ surface (Figure 4c). The observed quenching of the excited state could be attributed to an energy or electron transfer from the excited dye to the semiconductor [54,55], or more precisely, to the electron injection from the excited state of the dye into the conduction band of titanium dioxide (Figure 5). Although for $F_2POH@qTiO_2$ and $TPPS@qTiO_2$ the quenching process in the presence of $qTiO_2$ was not so evident, the observed slight decrease in fluorescence intensity may also indicate less effective electron/energy transfer processes (Figure 4).

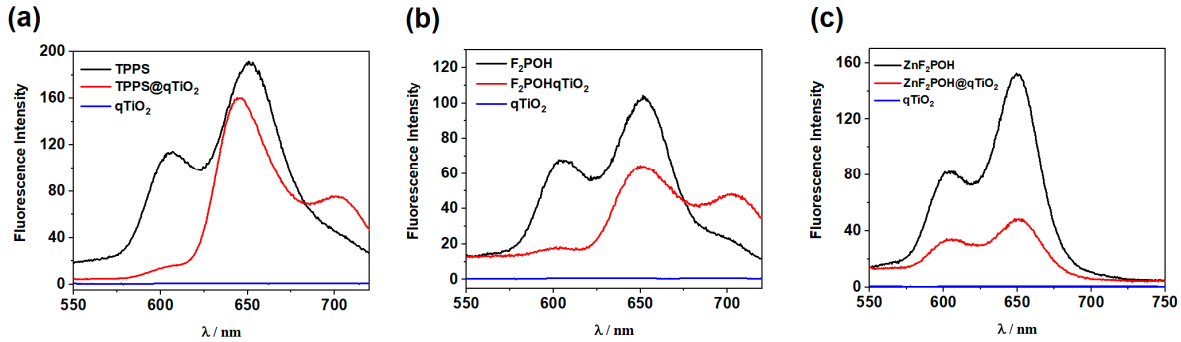

Figure 4. Fluorescence spectra of sulfonyl derivatives of porphyrins: (**a**) TPPS, (**b**) F_2POH, (**c**) ZnF_2POH, and relevant TiO_2-based nanomaterials.

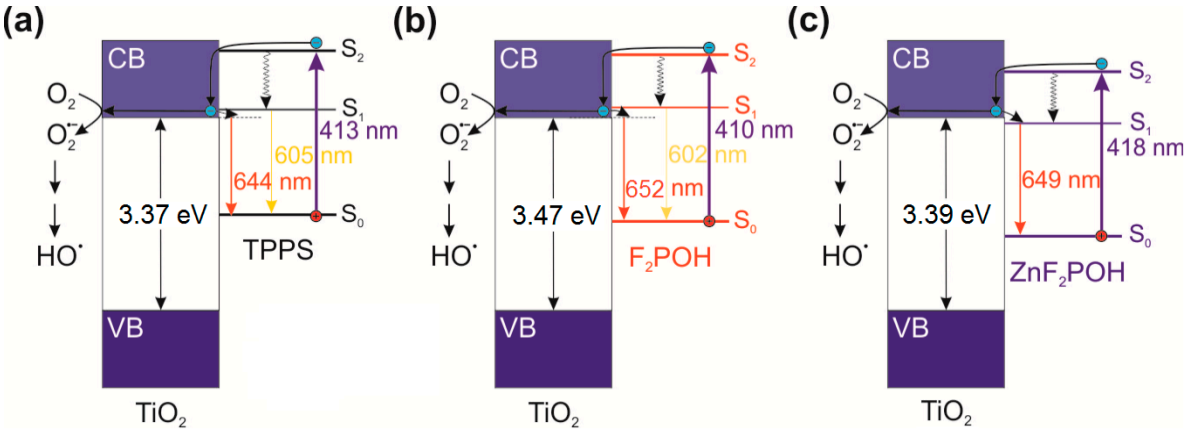

Figure 5. Proposed mechanism of the TiO_2 photosensitization, fluorescence emission, and possible pathway of hydroxyl radical generation after excitation of (**a**) $TPPS@qTiO_2$, (**b**) $F_2POH@qTiO_2$, and (**c**) $ZnF_2POH@qTiO_2$. CB—conduction band; VB—valence band.

The fluorescence quenching data clearly highlight the role of excited state of porphyrins in injecting their electron to the conduction band of $qTiO_2$. Additionally, the fluorescence intensity of porphyrin (Figure 4) decreased at a wavelength of ~600 nm and ~650 nm in the presence of $qTiO_2$. Meanwhile, the fluorescence intensity attributed to the interaction between $qTiO_2$ and porphyrin increased. An additional confirmation of this effect was the appearance of a new band at 700 nm (Figure 4, red line). The increase in the fluorescence lifetime of $porphyrin@qTiO_2$ compared to free porphyrin was the result of the emergence of a new relaxation path derived from the $qTiO_2$ surface modification by porphyrins (Figure 5).

Increasing the lifetime of an excited state correlated with reducing the recombination effectiveness. This effect was achieved through the transfer of the electron from the LUMO level of the porphyrin to the $qTiO_2$ conduction band. The presence of this mechanism was confirmed by the observed change in the fluorescence maxima for TPPS@$qTiO_2$ and F_2POH@TiO_2. In the case of ZnF_2POH@$qTiO_2$, the changes in the maximum were not observed, so the difference in lifetimes (twice longer) can be related with a different mechanism of relaxation of photoexcited electrons (see Figure 5c) or the possible geometry distortion of the porphyrin ring due to adsorption on $qTiO_2$. Moreover, the energy differences between fluorescence maxima for TPPS@$qTiO_2$ and F_2POH@$qTiO_2$ were about 0.14 eV, which suggests that the S_1 state of these porphyrins (in contrary to ZnF_2POH@$qTiO_2$) was located at higher energy than for the conduction band of $qTiO_2$. Thus, the oxygen-centered radical formation may have been promoted and the reduction of molecular oxygen to $O_2^{\bullet -}$ and further $HO^{\bullet}$ may have been preferred over that of ZnF_2POH@$qTiO_2$. Nevertheless, the mechanisms of ROS generation on the basis of the excitation of porphyrins themselves should also be considered. As indicated in Table 2, investigated porphyrins were characterized by different singlet oxygen quantum yield (Φ_Δ). Φ_Δ values were strongly affected by the substitution pattern and show the following trend: TPPS ≈ F_2POH < ZnF_2POH, with respective values of 0.64, 0.65, and 0.85, respectively [9]. The increase in Φ_Δ may be related to fluorine atoms substitution, as well as to metal insertion. The improvement of Φ_Δ by about 25% for ZnF_2POH suggests that this photosensitizer acted particularly through a type II photochemical mechanism. Consequently, after impregnation of studied porphyrins on the $qTiO_2$ surface, the prepared hybrid nanomaterials may generate both singlet oxygen as well as oxygen-centered radicals, which may improve the overall photochemical properties influencing the photodynamic activity of the photosensitizer [45].

2.3. Photoelectrochemical Properties of qTiO$_2$ Material

TiO_2 was characterized by the wide-band gap, hence the photoelectrochemical response upon irradiation was observed in the range of 300–400 nm (Figure 6), whereas for all porphyrin-based nanomaterials, the photocurrents appeared to be above 400 nm. These results confirm directly the photosensitization of TiO_2 with porphyrins within the visible light and are consistent with all spectroscopic data described above (including the mechanisms proposed in Figure 5). Moreover, the higher the photocurrent was, the more sufficient interfacial electron transfer (IFET) occurred. Therefore, the higher photocurrent value at 420 nm for F_2POH@$qTiO_2$, compared with others, clearly indicated that F_2POH@$qTiO_2$ seemed to be the most photoactive material upon irradiation. Other materials, such as ZnF_2POH@$qTiO_2$ and TPPS@$qTiO_2$, should be slightly less active in the IFET process above 400 nm. It is worth noting that bare $qTiO_2$ showed no photocurrent in this range. In addition, especially for ZnF_2POH@TiO_2 material, the activity of bare $qTiO_2$ in the UV range was not diminished [56,57], but increased significantly.

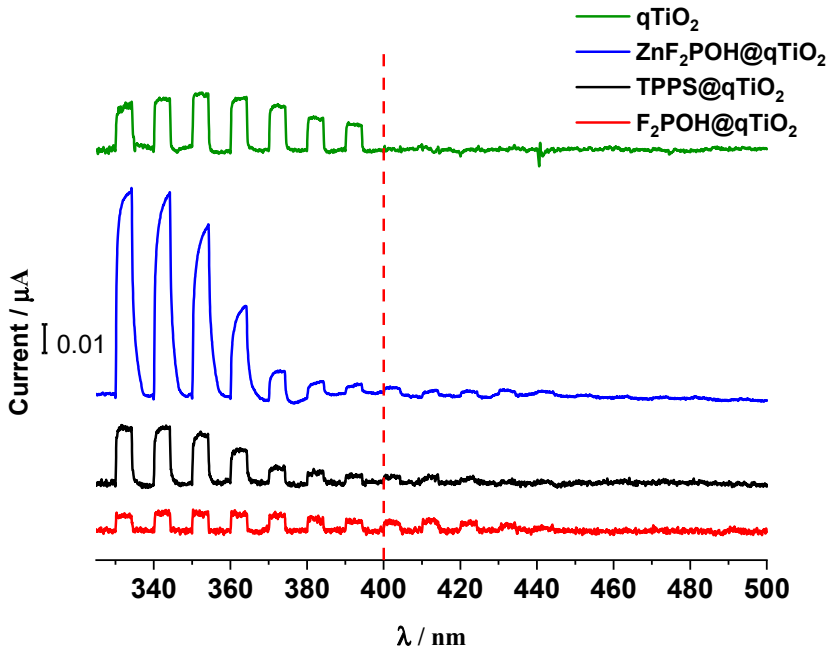

Figure 6. The photocurrent measurements as a function of the wavelength of incident light for sulfonated porphyrin (TPPS) and halogenated derivatives $F_2POH@qTiO_2$, $ZnF_2POH@qTiO_2$ adsorbed at the surface of TiO_2, as well as bare $qTiO_2$ as reference at the potential of 1000 mV vs. Ag/AgCl.

2.4. ROS Detection by Molecular Fluorescent Probes

To elucidate the activity of the porphyrin@$qTiO_2$ nanomaterials, several fluorescent probes for detection of various ROS were used. Photocurrents clearly confirmed electron transfer from the excited dye molecule to the conduction band of $qTiO_2$. Titanium dioxide (especially anatase polymorphs) appeared to be a strong oxidant. Its photo-excitation in water resulted in efficient $HO^{\bullet}$ generation as a result of water or surface hydroxyl group oxidation [58]. The 3-p-(hydroxyphenyl)fluorescein (HPF) probe, which possesses reasonable selectivity to hydroxyl radicals, shows that attaching (metallo)porphyrin to $qTiO_2$ led to an increased level of $HO^{\bullet}$ generation (Figure 7). In the case of TPPS, which is a well-known type II PS, generation of $HO^{\bullet}$ was also observed upon attachment to $qTiO_2$. The experiment performed with 3-p-(aminophenyl)fluorescein (APF) also confirmed an increasing level of ROS generation after impregnation of $qTiO_2$ with studied porphyrins. As shown in Figure 5, photoexcited electrons were transferred to the CB of titania. Electrons from the conduction band of TiO_2 may reduce the molecular oxygen adsorbed at the semiconductor surface in one- or three-electron processes to superoxide anion ($O_2^{\bullet-}$) or hydroxyl radicals, respectively. Such a mechanism has been reported several times by other authors [59]. For superoxide ion generated upon irradiation of the studied colloids, the dihydroethidium (DHE) probe was used (Figure 8). Moreover, to detect singlet oxygen in the studied systems, the Singlet Oxygen Sensor Green (SOSG) probe was also applied (Figure 8). The observed increase in the specific fluorescence signal for each probe proved that both singlet oxygen and oxygen-centered radicals were generated, and that the changes indicate the relative contribution of these ROS. This is especially important because by combining multiple mechanisms of ROS generation into a single material, the possibility of overcoming multidrug resistance is more likely [20,60].

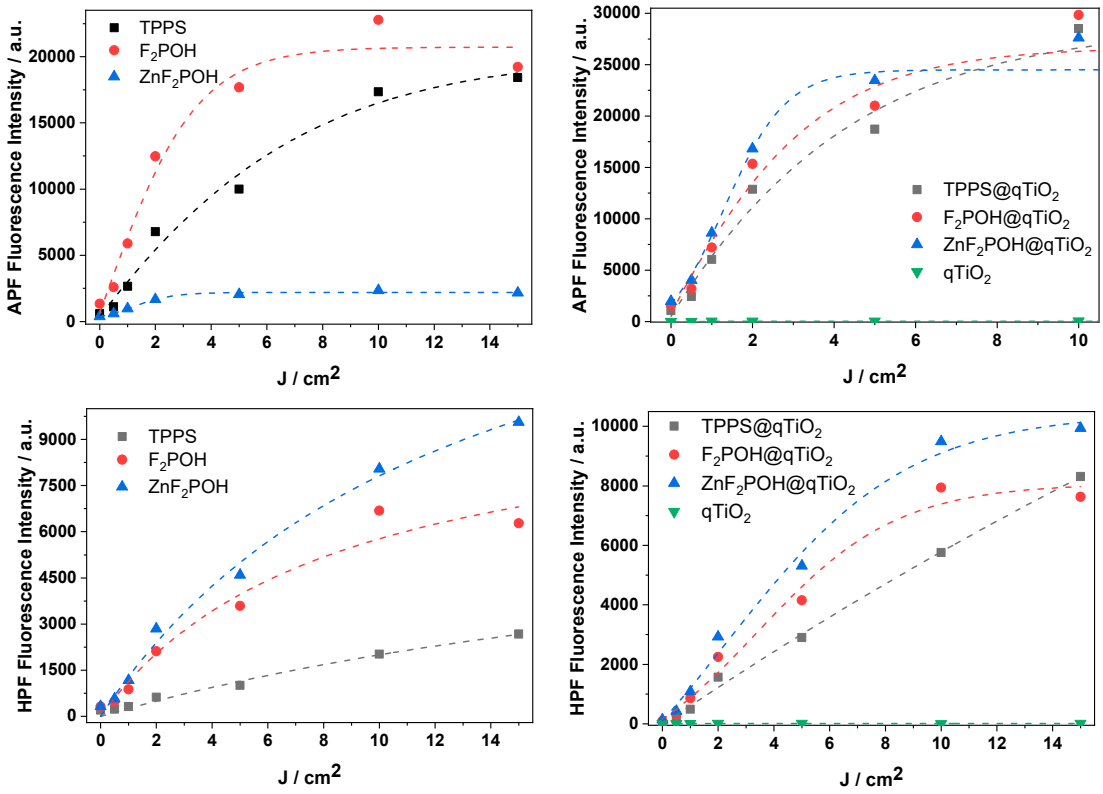

Figure 7. Photogeneration of reactive oxygen species (ROS). Light dose-dependent increase of fluorescence of fluorescent probes (10 μM): 3-p-(aminophenyl)fluorescein (APF), and 3-p-(hydroxyphenyl)fluorescein (HPF) in the presence of porphyrins and porphyrins at the surface of $qTiO_2$ materials irradiated with 420 ± 20 nm LED light.

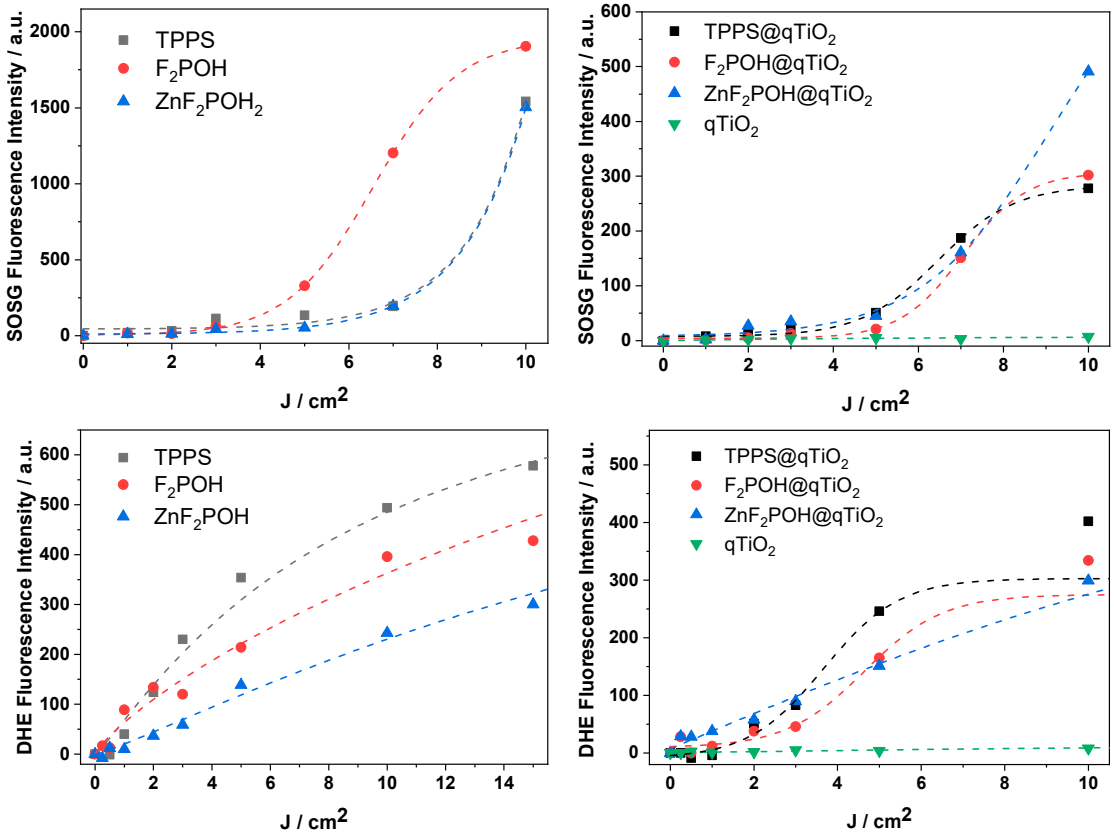

Figure 8. Photogeneration of ROS. Light dose-dependent increase of fluorescence of fluorescent probes (10 μM): dihydroethidium (DHE), and Singlet Oxygen Sensor Green (SOSG) in the presence of porphyrins and porphyrin-modified $qTiO_2$ materials irradiated with 420 ± 20 nm LED light.

2.5. Antimicrobial Studies

Upon visible light irradiation, porphyrin-based nanomaterials seemed to exhibit antimicrobial activity at a very low concentration (Figure 9). Unmodified $qTiO_2$ at a concentration of 1 g/L exhibited a killing efficacy of one log reduction due to the low absorption in visible light about 400 nm and 2 logs after potentiation with H_2O_2 or KI addition. Materials modified with porphyrin derivatives showed improved phototoxicity against both studied bacterial strains in a broad spectrum of applied concentrations, short-term incubation (2 h), and irradiation with 10 J/cm^2. Increased concentrations of materials caused further decrease in bacterial survival. In the case of photodynamic treatment without any potentiation (H_2O_2 or KI), the performed strategy reduced the colony forming unit (CFU) value at 1 g/L concentration of each material up to 3–4 logs. The most potent antibacterial effect was observed for $F_2POH@qTiO_2$. However, the complete bactericidal effect was not achieved in any case. Thus, for potentiation of PDI treatment, we performed the treatment with 100 mM H_2O_2 or 100 mM KI added to cells before irradiation. For all experimental groups we observed a huge potentiation of photodynamic effect with 2–4 additional logs in bacterial killing. A complete eradication of *Escherichia coli* was achieved for $TPPS@qTiO_2$_PDI + H_2O_2 at a concentration of 0.5 g/L, for $F_2POH@qTiO_2$ PDI + H_2O_2 and PDI + KI at 1g/L, and PDI + H_2O_2 for $ZnF_2POH@qTiO_2$ at 0.5 g/L. This had a great advantage over traditional methods, which usually do not lead to the complete destruction of *Escherichi coli* because the outer membrane of Gram-negative bacteria inhibits the uptake of drugs and antibiotics. The huge potentiation of PDI combined with H_2O_2 may be related to the increased amount of ROS, which was generated during PDI. The *Staphylococcus aureus* eradication was obtained only after using materials based on halogenated porphyrins (F_2POH and ZnF_2POH) that used ten times lower material concentration equal to 0.1 g/L after PDI with both H_2O_2 and KI

potentiation. In TPPS@qTiO$_2$-PDI combined with hydrogen peroxide or KI, the CFU notably decreased (1 log after H_2O_2 addition and 2 additional logs after KI) compared to the TPPS alone. Nevertheless, the bactericidal effect was not observed. Thus, F_2POH@qTiO$_2$ and ZnF_2POH@qTiO$_2$ exhibited a higher antimicrobial activity than TPPS@qTiO$_2$, which may have been related to fluorine atom substitution. Introduction of halogens into the macrocycle not only efficiently improved the photophysical properties of photosensitizers, but also their bioavailability biological activity [25,44].

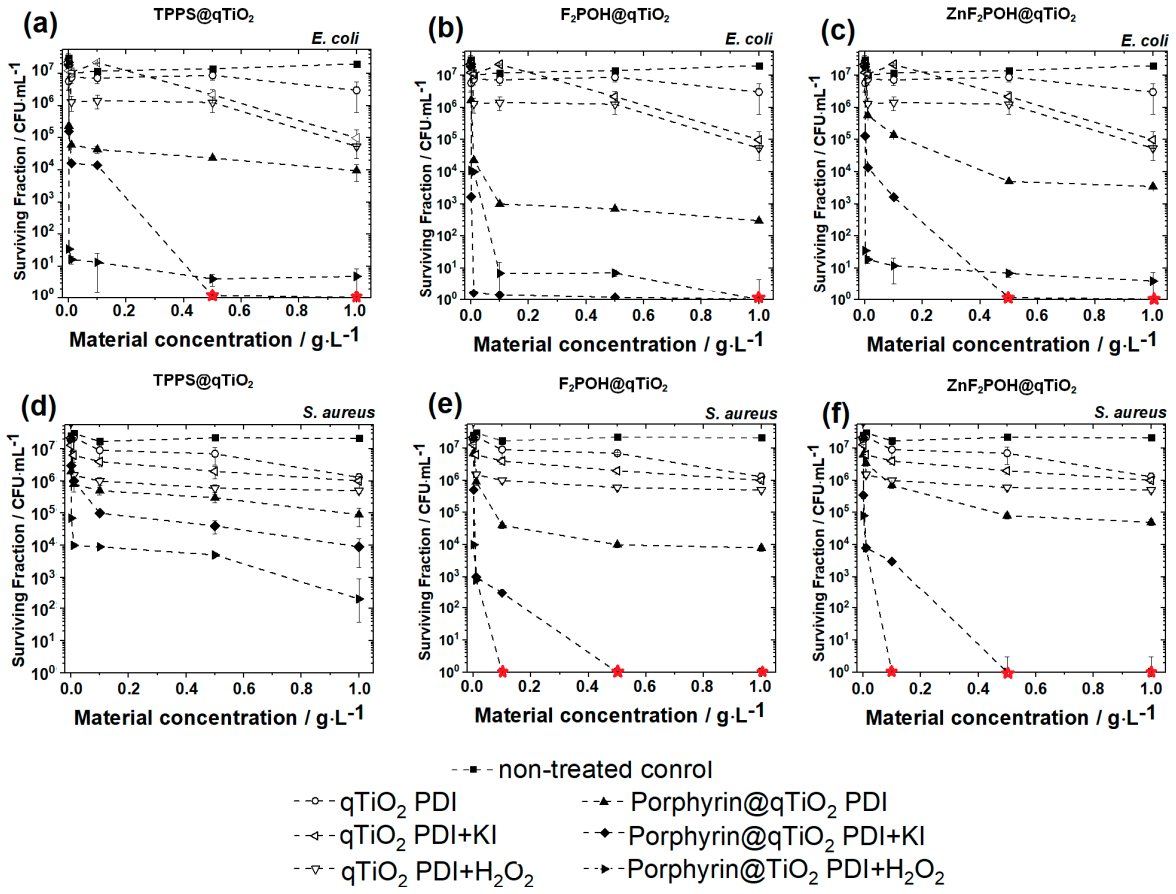

Figure 9. Photodynamic inactivation of *Escherichia coli* (**a**–**c**) and *Staphylococcus aureus* (**d**–**f**) mediated by qTiO$_2$-based hybrid materials (TPPS@qTiO$_2$, F_2POH@qTiO$_2$, and ZnF_2POH@qTiO$_2$) and with addition of KI (100 mM) or H_2O_2 (100 mM) after 2 h incubation and irradiated with 420 ± 20 nm LED light. Red symbols indicate the conditions required for complete bacteria eradication. Presented data are expressed as mean value ± SD.

2.6. Bacteria Imaging by Scanning Electron Microscopy (SEM) and Confocal Laser Scanning Microscopy (CLSM)

To visualize the photoinduced damages and the differences in the mechanisms of bacterial death, we performed SEM imaging immediately after each scheme of PDI treatment (PDI alone, PDI in combination with H_2O_2, and with KI, separately). The SEM images of *Escherichia coli* and *Staphylococcus aureus* are shown in Figures 10 and 11, and Figures S4 and S5. As may be observed, the PDI (incubation time: 2 h, material concentration of 0.5 g/L and light dose of 10 J/cm^2) against *Escherichia coli* indicated a bacteriostatic effect and may inhibit the bacteria division without visible membrane disruption. Nevertheless, it is believed that these bacteria were dying or losing cell functions with the intact cell walls. In contrast, after addition of 100 mM H_2O_2, the cells showed a substantially damaged cell membrane. In the case of PDI with addition of 100 mM KI, even more severe damage can be

observed (Figure 10). The membrane appeared to be "shredded" and the cells showed leakage of cellular contents.

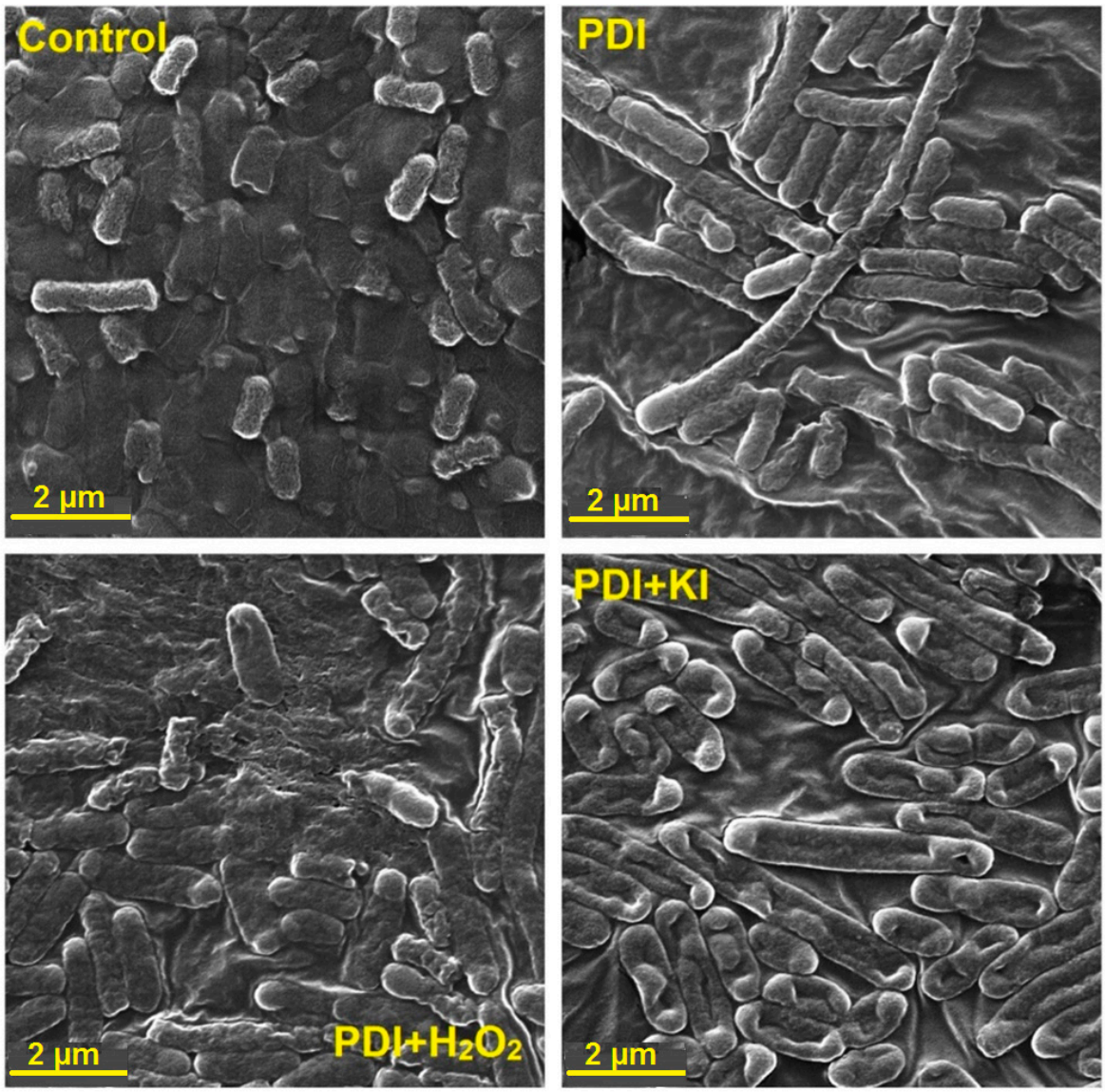

Figure 10. SEM images of *Escherichia coli* before PDI treatment (control) and bacterial cell debris after different PDI procedures (2 h incubation, 10 J/cm^2, 420 ± 20 nm LED light, material concentration of 0.5 g/L with addition of 100 mM H_2O_2 or 100 mM KI).

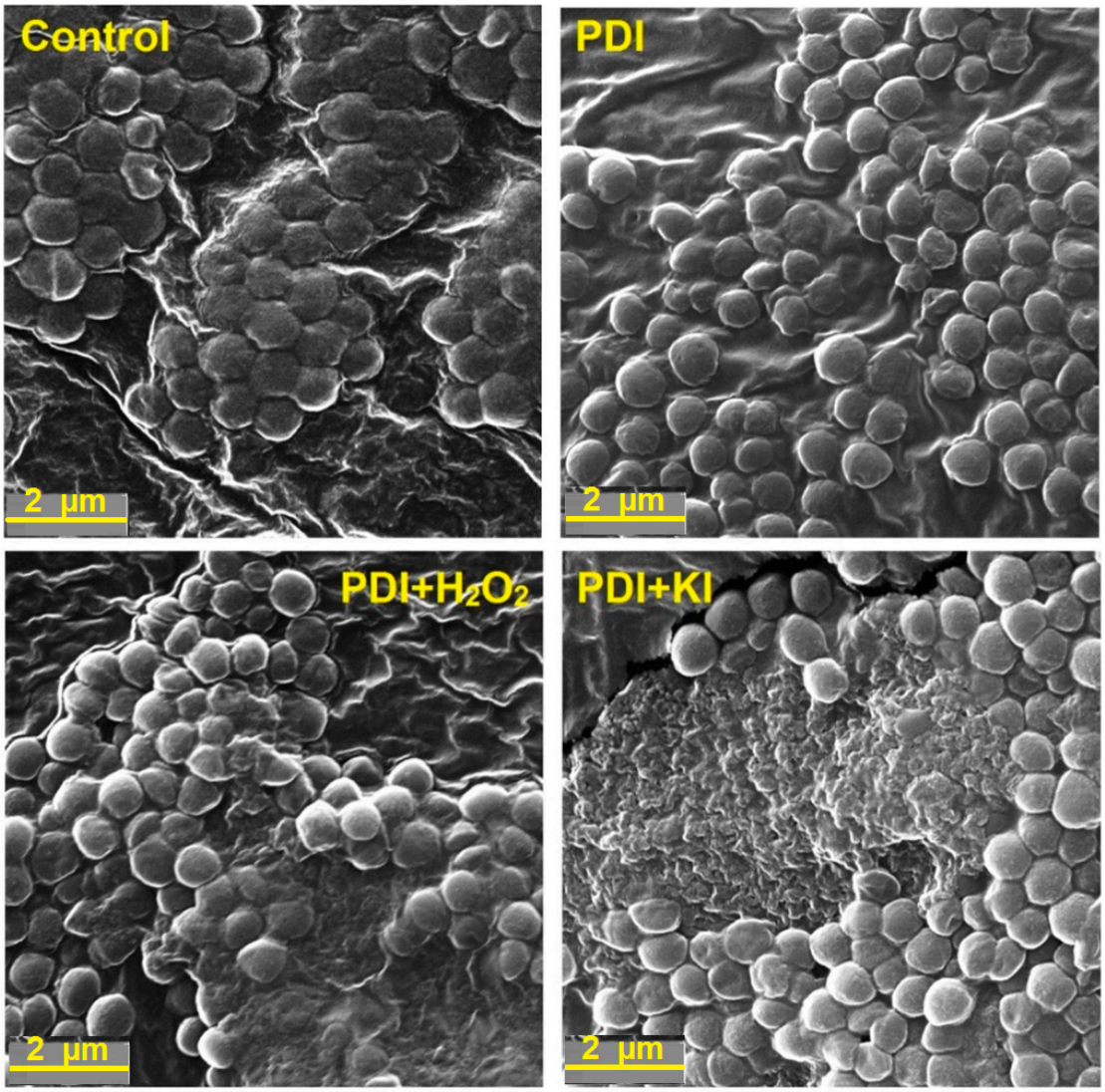

Figure 11. SEM images of *Staphylococcus aureus* before PDI treatment (control) and bacterial cell debris after different PDI procedures (2 h incubation, 10 J/cm^2, 420 ± 20 nm LED light, material concentration at 0.5 g/L with addition of 100 mM H_2O_2 or 100 mM KI).

Seemingly, a distant type of photodamage may have been detected for *Staphylococcus aureus* after PDI-treatment. Independently from the type of potentiation, the cells that received PDI with addition of 100 mM H_2O_2 or KI were killed completely (Figure 11). The images show multiple wall debris or even the area of completely disrupted cells. After the PDI-treatment alone, only cell shrinkage and gradual shape change were observed, whereas the application of the PDI treatment with H_2O_2 and KI led to a more pronounced effect.

However, because of the fact that the SEM images displayed similar structure of bacteria (in some cases only shapes were interrupted) we confirmed the presence of damaged cells by staining them with Hoechst33342 and propidium iodide (PI) (LIVE/DEAD staining) and imaging with CLSM. Figure 12 shows the images of untreated and photodynamically treated *Escherichia coli* and *Staphylococcus aureus* (incubation time: 2 h, material concentration of 0.5 g/L and light dose of 10 J/cm^2). The blue fluorescence signal is characteristic for intact living cells. In contrast, the red signal from PI clearly indicated that after PDI treatment, treated cells lost their integrity that allowed the dye (that is excluded by viable cells) to penetrate the cell membranes of disrupted or dead bacterial cells.

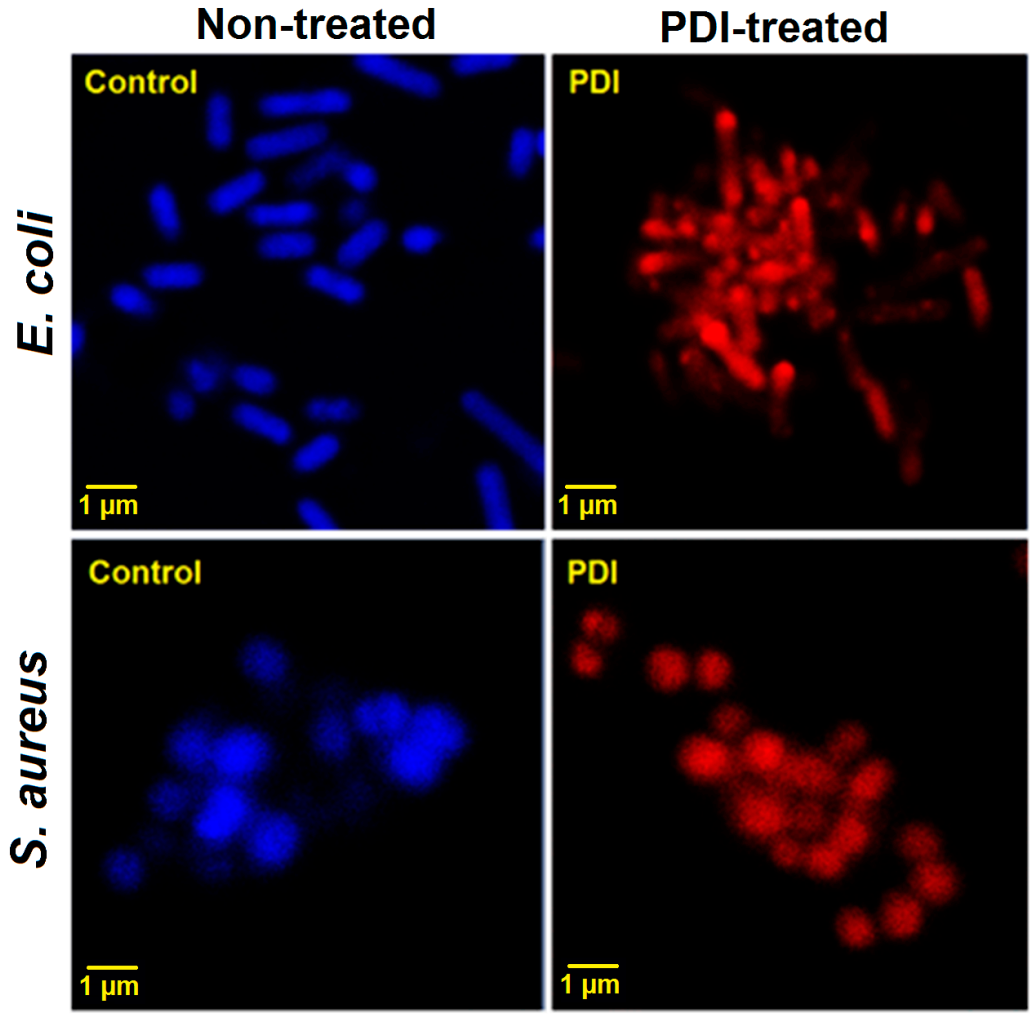

Figure 12. Laser scanning confocal microscopy images of non-treated and PDI treated (2 h incubation, 10 J/cm^2, 420 ± 20 nm LED light, material concentration at 0.5 g/L) *Escherichia coli* and *Staphylococcus aureus* stained with Hoechst33342 (live, blue fluorescence) and PI (dead, red fluorescence).

3. Discussion and Conclusions

Inorganic semiconductor photocatalysts offer a number of opportunities for environmental and biomedical applications. Particular attention has been given to titanium dioxide because of its unique properties, such as it being a wide-bandgap semiconductor, its non-toxicity to living organisms, its stability in water, and its strong photocatalytic activity when its crystal grain size is reduced to tenths of nanometers. Most importantly, it is also possible to modify its surface by many inorganic and organic molecules, and thus obtain hybrid materials that are able to extend the photoactivity of bare TiO_2 into the visible spectrum of light [9,10,42,45]. Our studies reveal that surface modification of qTiO_2 with commercially available TPPS and its fluorinated derivatives, F_2POH and ZnF_2POH, in aqueous medium at pH = 6 demonstrate efficient charge injection into the conduction band. This effect was confirmed by photocurrent measurements and steady-state fluorescence, as well as detection of a high amount of photogenerated ROS. Moreover, our photocatalysts based on highly-dispersed nanocolloidal TiO_2 were very efficient in the sensitization of semiconductor bandgap by interfacial charge-transfer transition (IFET). In contrast to TPPS in a homogeneous system, we demonstrated that prepared hybrid nanomaterials were able to generate not only singlet oxygen (as with free porphyrins in a homogeneous system), but also oxygen-centered radicals. Thus, their photoactivity was derived from multiple mechanisms of ROS generation. In fact, the ability of nanomaterials to facilitate electron transfer, and

thereby promote ROS generation, is a fundamental property of these materials and guarantees their use as an efficient photocatalyst in antimicrobial treatment. Our data clearly show that the modification of the $qTiO_2$ surface led to the presence of partition of hydroxyl radicals' generation, which was associated with the physicochemical characteristics in terms of both mechanisms and activity.

Efficient ROS generation is considered a key factor in sufficient photocatalysis and photodynamic inactivation of bacteria [25]. We have demonstrated that the nanomaterials synthesized and characterized by us are promising antimicrobial agents. We have also studied the PDI potentiation with H_2O_2 and KI to achieve complete eradication of pathogens. When KI was added, there was a huge increase in bacterial killing, ranging from 2 logs extra at 0.01 g/L, to >6 logs extra at 1 g/L in CFU reduction of *Escherichia coli* and *Staphylococcus aureus* after blue-light irradiation at a dose of 10 J/cm^2. It can be hypothesized that hydrogen peroxide would improve the efficacy of the performed PDI-treatment against *Escherichia coli* and *Staphylococcus aureus*, as the antibacterial photodynamic effect was improved across a wide concentration range of prepared materials at a low concentration of H_2O_2. It can also be suggested that H_2O_2 could increase the amount of ROS, which are generated during PDI [61]. However, some authors reported that the in vitro production of ROS did not increase in the presence of H_2O_2, meaning that the synergetic effect of H_2O_2 in PDT has another mechanism [62]. McCullagh et al. suggested the quenching of triplet-excited methylene blue by H_2O_2 in a type I process during PDT against *Synechococcus leopoliensis* [63]. In addition, hydrogen peroxide provides photodamage of bacterial membranes and increased drug accumulation in the cells [64]. The presence of H_2O_2 outside the bacteria facilitates the diffusion of PS into the bacteria [61,62]. Accordingly, for PDI combined with KI, the mechanism of action has been recently described [65–68]. In this case, the potentiation is caused by the formation of long-lived antimicrobial species (probably hypoiodite and iodine) in the reaction mixture (detected by adding bacteria after light), as well as short-lived antibacterial reactive species (bacteria present during light) able to produce more killing [67]. Hamblin et al. also reported that the potentiation of TiO_2-based materials in combination with UVA light, along with the presence of iodide, produces reactive iodine intermediates during illumination that kills microbial cells, and long-lived oxidized iodine products that kill after the application of light has ended [65].

Taken together, all of the performed studies indicate that TiO_2 nanoparticles modified with tetrapyrrolic compounds are an inorganic photoactive material with superior biological activity. Their antimicrobial properties in vitro in bacteria suspensions reveal that they are worth further investigation, especially in vivo in wound-healing processes and the elimination of localized infections.

4. Materials and Methods

4.1. Chemicals

Nanocrystalline TiO_2 (aqueous anatase colloid from Plasmachem, TiO_2 concentration of 5% [cat. PL-TiO-5p], average particle size of ca. 7 nm) was modified with porphyrins derivatives. Commercially available *meso*-tetra(4-sulfonatophenyl)porphyrin (TPPS) was obtained as the tetrasodium salt from Sigma-Aldrich. 5,10,15,20-Tetrakis(2,6-dibuorosulfonylophenyl) porphyrin (F_2POH) and its zinc(II) complex (ZnF_2POH) were prepared according to reported procedures [45,69,70].

4.2. Porphyrins@qTiO$_2$ Materials Preparation

In our experiments, 5% colloidal solution of TiO_2 nanoparticles in water was used and mixed with the water solution of a modifier (100 μM) in the ratio of 1:1 (*v*/*v*). In this way, color colloids of surface modified nanocrystalline TiO_2 were obtained. The pH of resulting colloid solution was adjusted with addition of 1% HCl solution to natural skin pH = 6. The solution was placed in a dialysis tube (Sigma, cut-off 14 kDa) and dialyzed two times against water in order to remove all low molecular-weight additives and the unbound modifier. Within this paper, the abbreviations TPPS@$qTiO_2$, F_2POH@$qTiO_2$, and ZnF_2POH@$qTiO_2$ have been assigned to modified colloids.

4.3. UV/VIS Electronic Absorption and Emission Spectra Measurements

UV/VIS absorption spectra were recorded with the Hewlett Packard HP8453 spectrophotometer in a 1 cm quartz cuvette. Fluorescence emission spectra were recorded from 550 to 750 nm with excitation at the Soret band (420 nm) using a Perkin Elmer Fluorescence Spectrometer LS 55.

4.4. Dynamic Light Scattering (DLS) and Zeta Potential Measurements

Zeta potential and hydrodynamic diameter measurements of nanomaterials in colloid materials were performed using Zetasizer Nano ZS (Malvern Instruments). The apparent diffusion coefficients of the nanoparticles were obtained from the normalized time correlation function of the scattered electric field, g(1)(τ), using the cumulants analysis. An average value was obtained from repeated measurements for each sample (N = 3).

4.5. Photoelectrochemical Measurements

Photocurrents of modified and unmodified $qTiO_2$ were measured using a three-electrode setup using 0.1 M solution of KNO_3 as electrolyte. The working electrode was prepared by spreading an aqueous suspension of studied material on ITO-coated transparent foil (60 Ω/sq resistance, Sigma-Aldrich) and dried afterwards in the stream of warm air (ca. 50 °C). A platinum wire and $Ag/AgCl_{(3M)}$ were used as the counter and reference electrodes, respectively. Photoelectrochemical measurements were performed using the photoelectric spectrometer (Instytut Fotonowy). The working electrodes were irradiated in the range of 330–500 nm from the backside through the ITO layer in order to minimize the influence of the film thickness on the measured photocurrents.

4.6. Characterization of Porphyrin@$qTiO_2$ Materials Using Scanning Electron Microscopy (SEM)

The morphologies and nanostructure of unmodified $qTiO_2$ and modified Porphyrin@$qTiO_2$ materials—TPPS@$qTiO_2$, F_2POH@$qTiO_2$ and ZnF_2POH@$qTiO_2$—were examined by scanning electron microscope Vega 3 (Tescan) equipped with LaB6 cathode, operated at a voltage of 30 kV.

4.7. Detection of Reactive Oxygen Species Using Fluorescent Probes

3-p-(Aminophenyl)fluorescein (APF) and 3-p-(hydroxyphenyl)fluorescein (HPF) are selective probes for oxygen reduction products. Singlet Oxygen Sensor Green (SOSG) is a specific probe for singlet oxygen, whereas dihydroethidinum (DHE) traps superoxide ion. These probes were employed for the detection of ROS generated during illumination of the colloid materials with absorbance at the same level at about 1.0. Each fluorescent probe was added to a well at a final concentration of 10 μM. Freshly prepared solutions were then irradiated with LED (420 ± 20 nm) light for increasing time-intervals. A microplate reader (Tecan Infinite M200 Reader) was used for acquisition of fluorescence signal immediately before and after illumination. When APF and HPF were employed, fluorescence emission at 515 nm was acquired upon excitation at 490 nm. With SOSG, the corresponding values were 525 and 505 nm, and for DHE, 480 nm and 580 nm, respectively [25].

4.8. Photodynamic Inactivation (PDI) of Bacteria

The microorganisms used in PDI were *Escherichia coli* (K12) and *Staphylococcus aureus* (8325–4). The planctonic *Escherichia coli* were cultured in Luria Broth (LB) (BioShop Lab Science Products) and *Staphylococcus aureus* in brain heart infusion broth (BHI) (Sigma-Aldrich) in an orbital incubator (37 °C, 130 rpm) until the optical density reached OD = 0.5, which corresponds to approximately 10^7 CFU per mL. For PDI experiments, suspensions of bacteria were incubated with various concentrations of hybrid nanomaterials for 2 h in the dark at room temperature. For further potentiation effect, in other experimental groups, bacteria were also incubated with the addition of 100 mM H_2O_2 or 100 mM KI. Then, aliquots (1 mL) were transferred to a 12-well plate and illuminated with a blue light. We used blue-LED array (420 ± 20 nm) to deliver a light dose of 10 J/cm^2 (measured with a radiometer).

After illumination (or dark incubation), samples were resuspended, diluted in water, mixed and plated (LB or BHI agars). Aliquots were taken from each well to determine the CFU value. Plates were segregated in triplicate and incubated for 24 h at 37 °C in the dark to allow colony formation. A control group of bacterial cells treated with light showed the same number of CFU as the absolute control (data not shown). The viability of bacteria was also monitored using LIVE/DEAD BacLight Bacterial Viability Kit (Invitrogen; monitors membrane integrity) according to the manufacturer's instructions. All values were expressed as average ± SD (standard deviation), which represented the standard deviation of the sample mean estimate of a population mean.

4.9. CLSM Fluorescence Imaging of Bacteria

Bacterial viability and photodynamically-induced damages were followed with fluorescence confocal imaging using a Zeiss LSM880 laser-scanning microscope equipped with an argon ion laser. The objective used was a water-immersion objective lens (63×, Carl Zeiss Ltd.) with a working distance of 1.46 mm. Selected bacteria were incubated with the photosensitizer and irradiated accordingly to the PDI protocol described above. Then, bacteria were stained with two nucleic acid dyes: propidium iodide (PI) to stain dead bacteria and Hoechst33342, which is able to stain only bacteria with an intact membrane (living). After washing, the microorganism cells were placed on the microscopic glass slides and imaged. Registered images were analyzed with the Zeiss ZEN software.

4.10. Statistics

All values were expressed as average ± SD (standard deviation), which represented the average squared deviation from the mean. All experiments were repeated at least three times with comparable results. The sample size in biological tests was N = 6–12 in each experimental group.

Supplementary Materials: The following are available online at Available online: www.mdpi.com/xxx/s1 (accessed on 8 May 2012).: Figure S1: Absorption spectra of $qTiO_2$ and the calculation of the band gaps based on the Tauc plot with baseline correction. Figure S2: SEM images of nanostructured $qTiO_2$, TPPS@$qTiO_2$, F_2POH@$qTiO_2$ and ZnF_2POH@TiO_2 recorded on carbon tape with size of particle highlighted. Figure S3: SEM images of nanostructured $qTiO_2$, TPPS@$qTiO_2$, F_2POH@$qTiO_2$, and ZnF_2POH@TiO_2 recorded on carbon tape with size of particle highlighted. Figure S4: SEM images of *Escherichia coli* before PDI treatment (control) and bacterial cells debris after different PDI procedures. Figure S5: SEM images of *Staphylococcus aureus* before PDI treatment (control) and bacterial cells debris after different PDI procedures.

Author Contributions: Conceptualization, J.M.D.; methodology, A.S., B.P., M.K., P.Ł., and J.M.D.; formal analysis, A.S., B.P., M.K., and J.M.D.; investigation, A.S., B.P., M.K., and J.M.D.; resources, G.D. and J.M.D.; data curation, A.S., B.P., and M.K.; Writing—Original draft preparation, A.S., B.P., M.K., and J.M.D.; Writing—Review and editing, A.S., B.P., P.Ł., and J.M.D.; visualization, A.S., B.P., and M.K.; supervision, J.M.D.; project administration, J.M.D.; funding acquisition, G.D., P.Ł., and J.M.D.

Funding: The work was the result of the implementation of the research project (Sonata Bis) number 2016/22/E/NZ7/00420 given to JMD funded by the National Science Center (NCN), Poland.

Acknowledgments: B.P. thanks the Foundation for Polish Science (FNP) for the START 071.2019 program. M.K. acknowledges the support by the Foundation for Polish Science (FNP) within the TEAM Project (POIR.04.04.00-00-3D74/16). P.Ł. thanks the NCN for the Sonata grant No. 2016/21/D/NZ7/00611. Some of the research was carried out with equipment purchased with the financial support of the European Regional Development Fund in the framework of the Polish Innovation Economy Operational Program (contract No. POIG.02.01.00-12-167/08, project Malopolska Centre of Biotechnology).

Conflicts of Interest: The authors declare no conflict of interest.

References

1. Zouzelka, R.; Remzova, M.; Plsek, J.; Brabec, L.; Rathousky, J. Immobilized rGO/TiO_2 Photocatalyst for Decontamination of Water. *Catalysts* **2019**, *9*, 708. [CrossRef]
2. Oszajca, M.; Brindell, M.; Orzeł, Ł.; Dąbrowski, J.M.; Śpiewak, K.; Łabuz, P.; Pacia, M.; Stochel-Gaudyn, A.; Macyk, W.; van Eldik, R. Mechanistic studies on versatile metal-assisted hydrogen peroxide activation processes for biomedical and environmental incentives. *Coord. Chem. Rev.* **2016**, *327*, 143–165. [CrossRef]

3. Kočí, K.; Reli, M.; Troppová, I.; Šihor, M.; Kupková, J.; Kustrowski, P.; Praus, P. Photocatalytic decomposition of N_2O over TiO_2/g-C_3N_4 photocatalysts heterojunction. *Appl. Surf. Sci.* **2017**, *396*, 1685–1695. [CrossRef]
4. Falkowski, M.; Rebis, T.; Kryjewski, M.; Popenda, L.; Lijewski, S.; Jurga, S.; Mielcarek, J.; Milczarek, G.; Goslinski, T. An enhanced electrochemical nanohybrid sensing platform consisting of reduced graphene oxide and sulfanyl metalloporphyrazines for sensitive determination of hydrogen peroxide and L-cysteine. *Dyes Pigments* **2017**, *138*, 190–203. [CrossRef]
5. Sadowski, R.; Strus, M.; Buchalska, M.; Heczko, P.B.; Macyk, W. Visible light induced photocatalytic inactivation of bacteria by modified titanium dioxide films on organic polymers. *Photochem. Photobiol. Sci.* **2015**, *14*, 514–519. [CrossRef] [PubMed]
6. Lee, C.M.; Palaniandy, P.; Dahlan, I. Pharmaceutical residues in aquatic environment and water remediation by TiO_2 heterogeneous photocatalysis: A review. *Environ. Earth Sci.* **2017**, *76*, 611. [CrossRef]
7. Fagan, R.; McCormack, D.E.; Dionysiou, D.D.; Pillai, S.C. A review of solar and visible light active TiO_2 photocatalysis for treating bacteria, cyanotoxins and contaminants of emerging concern. *Mater. Sci. Semicond. Process.* **2016**, *42*, 2–14. [CrossRef]
8. Byrne, J.; Dunlop, P.; Hamilton, J.; Fernández-Ibáñez, P.; Polo-López, I.; Sharma, P.; Vennard, A. A review of heterogeneous photocatalysis for water and surface disinfection. *Molecules* **2015**, *20*, 5574–5615. [CrossRef]
9. Sułek, A.; Pucelik, B.; Kuncewicz, J.; Dubin, G.; Dąbrowski, J.M. Sensitization of TiO_2 by halogenated porphyrin derivatives for visible light biomedical and environmental photocatalysis. *Catal. Today* **2019**, *335*, 538–549. [CrossRef]
10. Regiel-Futyra, A.; Dąbrowski, J.M.; Mazuryk, O.; Śpiewak, K.; Kyzioł, A.; Pucelik, B.; Brindell, M.; Stochel, G. Bioinorganic antimicrobial strategies in the resistance era. *Coord. Chem. Rev.* **2017**, *351*, 76–117. [CrossRef]
11. Sobotta, L.; Skupin-Mrugalska, P.; Mielcarek, J.; Goslinski, T.; Balzarini, J. Photosensitizers mediated photodynamic inactivation against virus particles. *Mini Rev. Med. Chem.* **2015**, *15*, 503–521. [CrossRef] [PubMed]
12. Jori, G.; Brown, S.B. Photosensitized inactivation of microorganisms. *Photochem. Photobiol. Sci.* **2004**, *3*, 403–405. [CrossRef] [PubMed]
13. Donnelly, R.F.; McCarron, P.A.; Tunney, M.M. Antifungal photodynamic therapy. *Microbiol. Res.* **2008**, *163*, 1–12. [CrossRef]
14. Costerton, J.W.; Stewart, P.S.; Greenberg, E.P. Bacterial biofilms: A common cause of persistent infections. *Science* **1999**, *284*, 1318–1322. [CrossRef] [PubMed]
15. Maisch, T. Anti-microbial photodynamic therapy: Useful in the future? *Lasers Med. Sci.* **2007**, *22*, 83–91. [CrossRef]
16. Maisch, T.; Szeimies, R.-M.; Jori, G.; Abels, C. Antibacterial photodynamic therapy in dermatology. *Photochem. Photobiol. Sci.* **2004**, *3*, 907–917. [CrossRef] [PubMed]
17. Kawczyk-Krupka, A.; Pucelik, B.; Międzybrodzka, A.; Sieroń, A.R.; Dąbrowski, J.M. Photodynamic therapy as an alternative to antibiotic therapy for the treatment of infected leg ulcers. *Photodiagnosis Photodyn. Ther.* **2018**, *23*, 132–143. [CrossRef] [PubMed]
18. Dlugaszewska, J.; Szczolko, W.; Koczorowski, T.; Skupin-Mrugalska, P.; Teubert, A.; Konopka, K.; Kucinska, M.; Murias, M.; Düzgüneş, N.; Mielcarek, J. Antimicrobial and anticancer photodynamic activity of a phthalocyanine photosensitizer with N-methyl morpholiniumethoxy substituents in non-peripheral positions. *J. Inorg. Biochem.* **2017**, *172*, 67–79. [CrossRef]
19. Huang, L.; Xuan, Y.; Koide, Y.; Zhiyentayev, T.; Tanaka, M.; Hamblin, M.R. Type I and Type II mechanisms of antimicrobial photodynamic therapy: An in vitro study on gram-negative and gram-positive bacteria. *Lasers Surg. Med.* **2012**, *44*, 490–499. [CrossRef]
20. Dąbrowski, J.M. Reactive oxygen species in photodynamic therapy: Mechanisms of their generation and potentiation. In *Advances in Inorganic Chemistry*; Elsevier: Amsterdam, The Netherlands, 2017; Volume 70, pp. 343–394.
21. Martin, J.P.; Logsdon, N. The role of oxygen radicals in dye-mediated photodynamic effects in Escherichia coli B. *J. Biol. Chem.* **1987**, *262*, 7213–7219.
22. Alves, E.; Faustino, M.A.; Neves, M.G.; Cunha, Â.; Nadais, H.; Almeida, A. Potential applications of porphyrins in photodynamic inactivation beyond the medical scope. *J. Photochem. Photobiol. C Photochem. Rev.* **2015**, *22*, 34–57. [CrossRef]

23. Lopes, L.Q.S.; Ramos, A.P.; Copetti, P.M.; Acunha, T.V.; Iglesias, B.A.; Santos, R.C.V.; Machado, A.K.; Sagrillo, M.R. Antimicrobial activity and safety applications of meso-tetra (4-pyridyl) platinum (II) porphyrin. *Microb. Pathog.* **2019**, *128*, 47–54. [CrossRef] [PubMed]
24. Castro, K.A.; Moura, N.M.; Figueira, F.; Ferreira, R.I.; Simões, M.M.; Cavaleiro, J.A.; Faustino, M.A.F.; Silvestre, A.J.; Freire, C.S.; Tomé, J.P. New Materials Based on Cationic Porphyrins Conjugated to Chitosan or Titanium Dioxide: Synthesis, Characterization and Antimicrobial Efficacy. *Int. J. Mol. Sci.* **2019**, *20*, 2522. [CrossRef] [PubMed]
25. Pucelik, B.; Paczyński, R.; Dubin, G.; Pereira, M.M.; Arnaut, L.G.; Dąbrowski, J.M. Properties of halogenated and sulfonated porphyrins relevant for the selection of photosensitizers in anticancer and antimicrobial therapies. *PLoS ONE* **2017**, *12*, e0185984. [CrossRef] [PubMed]
26. Jiang, D.; Xu, Y.; Wu, D.; Sun, Y. Visible-light responsive dye-modified TiO_2 photocatalyst. *J. Solid State Chem.* **2008**, *181*, 593–602. [CrossRef]
27. Li, H.; Li, M.; Zhang, L.; Zhang, X.; Ma, Y.; Yu, B.; Wei, Q.; Yin, S. Dipyridylbenzene as a charming sensitizer to significantly enhance the photocatalytic activity of titanium dioxide. *Appl. Catal. B Environ.* **2018**, *232*, 472–480. [CrossRef]
28. Lord, M.S.; Foss, M.; Besenbacher, F. Influence of nanoscale surface topography on protein adsorption and cellular response. *Nano Today* **2010**, *5*, 66–78. [CrossRef]
29. Huang, Y.-Y.; Sharma, S.K.; Dai, T.; Chung, H.; Yaroslavsky, A.; Garcia-Diaz, M.; Chang, J.; Chiang, L.Y.; Hamblin, M.R. Can nanotechnology potentiate photodynamic therapy? *Nanotechnol. Rev.* **2012**, *1*, 111–146. [CrossRef]
30. Kozinska, A.; Zadlo, A.; Labuz, P.; Broniec, A.; Pabisz, P.; Sarna, T. The Ability of Functionalized Fullerenes and Surface-Modified TiO_2 Nanoparticles to Photosensitize Peroxidation of Lipids in Selected Model Systems. *Photochem. Photobiol.* **2019**, *95*, 227–236.
31. Mesquita, M.Q.; Dias, C.J.; Neves, M.P.M.S.; Almeida, A.; Faustino, M.F. Revisiting current photoactive materials for antimicrobial photodynamic therapy. *Molecules* **2018**, *23*, 2424. [CrossRef]
32. Hajipour, M.J.; Fromm, K.M.; Ashkarran, A.A.; de Aberasturi, D.J.; de Larramendi, I.R.; Rojo, T.; Serpooshan, V.; Parak, W.J.; Mahmoudi, M. Antibacterial properties of nanoparticles. *Trends Biotechnol.* **2012**, *30*, 499–511. [CrossRef] [PubMed]
33. Hamblin, M.R.; Hasan, T. Photodynamic therapy: A new antimicrobial approach to infectious disease? *Photochem. Photobiol. Sci.* **2004**, *3*, 436–450. [CrossRef]
34. Daniel, M.-C.; Astruc, D. Gold nanoparticles: Assembly, supramolecular chemistry, quantum-size-related properties, and applications toward biology, catalysis, and nanotechnology. *Chem. Rev.* **2004**, *104*, 293–346. [CrossRef] [PubMed]
35. Demidova, T.N.; Hamblin, M.R. Effect of cell-photosensitizer binding and cell density on microbial photoinactivation. *Antimicrob. Agents Chemother.* **2005**, *49*, 2329–2335. [CrossRef] [PubMed]
36. Hamblin, M.R. Potentiation of antimicrobial photodynamic inactivation by inorganic salts. *Expert Rev. Anti-Infect. Ther.* **2017**, *15*, 1059–1069. [CrossRef] [PubMed]
37. Łabuz, P.; Sadowski, R.; Stochel, G.; Macyk, W. Visible light photoactive titanium dioxide aqueous colloids and coatings. *Chem. Eng. J.* **2013**, *230*, 188–194. [CrossRef]
38. Arce-Sarria, A.; Machuca-Martínez, F.; Bustillo-Lecompte, C.; Hernández-Ramírez, A.; Colina-Márquez, J. Degradation and Loss of Antibacterial Activity of Commercial Amoxicillin with TiO_2/WO_3-Assisted Solar Photocatalysis. *Catalysts* **2018**, *8*, 222. [CrossRef]
39. Sakar, M.; Prakash, R.M.; Do, T.-O. Insights into the TiO_2-Based Photocatalytic Systems and Their Mechanisms. *Catalysts* **2019**, *9*, 680. [CrossRef]
40. Buchalska, M.; Łabuz, P.; Kuncewicz, J.; Macyk, W. Mechanism of the photocatalytic processes on titanium (IV) titanium (IV)-catecholate catecholate complexes complexes upon two colors irradiation. In Proceedings of the 7th European Meeting on Solar Chemistry and Photocatalysis: Environmental Applications—SPEA7, Oporto, Portugal, 17–20 June 2012.
41. Jańczyk, A.; Wolnicka-Głubisz, A.; Urbanska, K.; Kisch, H.; Stochel, G.; Macyk, W. Photodynamic activity of platinum (IV) chloride surface-modified TiO_2 irradiated with visible light. *Free Radic. Biol. Med.* **2008**, *44*, 1120–1130. [CrossRef] [PubMed]
42. Macyk, W.; Szaciłowski, K.; Stochel, G.; Buchalska, M.; Kuncewicz, J.; Łabuz, P. Titanium (IV) complexes as direct TiO_2 photosensitizers. *Coord. Chem. Rev.* **2010**, *254*, 2687–2701. [CrossRef]

43. Dąbrowski, J.M.; Pucelik, B.; Regiel-Futyra, A.; Brindell, M.; Mazuryk, O.; Kyzioł, A.; Stochel, G.; Macyk, W.; Arnaut, L.G. Engineering of relevant photodynamic processes through structural modifications of metallotetrapyrrolic photosensitizers. *Coord. Chem. Rev.* **2016**, *325*, 67–101. [CrossRef]
44. Pucelik, B.; Gürol, I.; Ahsen, V.; Dumoulin, F.; Dąbrowski, J.M. Fluorination of phthalocyanine substituents: Improved photoproperties and enhanced photodynamic efficacy after optimal micellar formulations. *Eur. J. Med. Chem.* **2016**, *124*, 284–298. [CrossRef]
45. Dąbrowski, J.M.; Pucelik, B.; Pereira, M.M.; Arnaut, L.G.; Stochel, G. Towards tuning PDT relevant photosensitizer properties: Comparative study for the free and Zn^{2+} coordinated meso-tetrakis [2,6-difluoro-5-(N-methylsulfamylo) phenyl] porphyrin. *J. Coord. Chem.* **2015**, *68*, 3116–3134. [CrossRef]
46. Regulska, E.; Rivera-Nazario, D.M.; Karpinska, J.; Plonska-Brzezinska, M.E.; Echegoyen, L. Zinc Porphyrin-Functionalized Fullerenes for the Sensitization of Titania as a Visible-Light Active Photocatalyst: River Waters and Wastewaters Remediation. *Molecules* **2019**, *24*, 1118. [CrossRef] [PubMed]
47. Stangel, C.; Schubert, C.; Kuhri, S.; Rotas, G.; Margraf, J.T.; Regulska, E.; Clark, T.; Torres, T.; Tagmatarchis, N.; Coutsolelos, A.G. Tuning the reorganization energy of electron transfer in supramolecular ensembles–metalloporphyrin, oligophenylenevinylenes, and fullerene–and the impact on electron transfer kinetics. *Nanoscale* **2015**, *7*, 2597–2608. [CrossRef]
48. Regulska, E.; Rivera-Nazario, D.M.; Karpinska, J.; Plonska-Brzezinska, M.E.; Echegoyen, L. Enhanced Photocatalytic Performance of Porphyrin/Phthalocyanine and Bis (4-pyridyl) pyrrolidinofullerene modified Titania. *ChemistrySelect* **2017**, *2*, 2462–2470. [CrossRef]
49. Carvalho, C.M.; Alves, E.; Costa, L.; Tomé, J.P.; Faustino, M.A.; Neves, M.G.; Tomé, A.C.; Cavaleiro, J.A.; Almeida, A.; Cunha, A.N. Functional cationic nanomagnet-porphyrin hybrids for the photoinactivation of microorganisms. *ACS Nano* **2010**, *4*, 7133–7140. [CrossRef] [PubMed]
50. Lauceri, R.; Gurrieri, S.; Bellacchio, E.; Contino, A.; Monsu'scolaro, L.; Romeo, A.; Toscano, A.; Purrello, R. J-Type Aggregates of the Anionic Meso-Tetrakis (4-Sulfonatophenyl) Porphine Induced by ‚Hindered'Cationic Porphyrins. *Supramol. Chem.* **2000**, *12*, 193–202. [CrossRef]
51. Dąbrowski, J.M.; Pucelik, B.; Pereira, M.M.; Arnaut, L.G.; Macyk, W.; Stochel, G. New hybrid materials based on halogenated metalloporphyrins for enhanced visible light photocatalysis. *RSC Adv.* **2015**, *5*, 93252–93261. [CrossRef]
52. Satoh, N.; Nakashima, T.; Kamikura, K.; Yamamoto, K. Quantum size effect in TiO_2 nanoparticles prepared by finely controlled metal assembly on dendrimer templates. *Nat. Nanotechnol.* **2008**, *3*, 106. [CrossRef]
53. Reddy, K.M.; Manorama, S.V.; Reddy, A.R. Bandgap studies on anatase titanium dioxide nanoparticles. *Mater. Chem. Phys.* **2003**, *78*, 239–245. [CrossRef]
54. Tachibana, Y.; Haque, S.A.; Mercer, I.P.; Durrant, J.R.; Klug, D.R. Electron injection and recombination in dye sensitized nanocrystalline titanium dioxide films: A comparison of ruthenium bipyridyl and porphyrin sensitizer dyes. *J. Phys. Chem. B* **2000**, *104*, 1198–1205. [CrossRef]
55. Nazeeruddin, M.K.; Péchy, P.; Renouard, T.; Zakeeruddin, S.M.; Humphry-Baker, R.; Cointe, P.; Liska, P.; Cevey, L.; Costa, E.; Shklover, V.; et al. Engineering of efficient panchromatic sensitizers for nanocrystalline TiO_2-based solar cells. *J. Am. Chem. Soc.* **2001**, *123*, 1613–1624. [CrossRef] [PubMed]
56. Qi, K.; Zasada, F.; Piskorz, W.; Indyka, P.; Grybos, J.; Trochowski, M.; Buchalska, M.; Kobielusz, M.; Macyk, W.; Sojka, Z. Self-Sensitized Photocatalytic Degradation of Colorless Organic Pollutants Attached to Rutile Nanorods Experimental and Theoretical DFT+ D Studies. *J. Phys. Chem. C* **2016**, *120*, 5442–5456. [CrossRef]
57. Sadowski, R.; Wach, A.; Buchalska, M.; Kuśtrowski, P.; Macyk, W. Photosensitized TiO_2 films on polymers–Titania-polymer interactions and visible light induced photoactivity. *Appl. Surf. Sci.* **2019**, *475*, 710–719. [CrossRef]
58. Kobielusz, M.; Pilarczyk, K.; Świętek, E.; Szaciłowski, K.; Macyk, W. Spectroelectrochemical analysis of TiO_2 electronic states–Implications for the photocatalytic activity of anatase and rutile. *Catal. Today* **2018**, *309*, 35–42. [CrossRef]
59. Buchalska, M.; Kobielusz, M.; Matuszek, A.; Pacia, M.; Wojtyła, S.; Macyk, W. On oxygen activation at rutile-and anatase-TiO_2. *ACS Catal.* **2015**, *5*, 7424–7431. [CrossRef]
60. Buchalska, M.; Łabuz, P.; Bujak, Ł.; Szewczyk, G.; Sarna, T.; Maćkowski, S.; Macyk, W. New insight into singlet oxygen generation at surface modified nanocrystalline TiO_2–the effect of near-infrared irradiation. *Dalton Trans.* **2013**, *42*, 9468–9475. [CrossRef]

61. Yang, S.M.; Lee, D.W.; Park, H.J.; Kwak, M.H.; Park, J.M.; Choi, M.G. Hydrogen Peroxide Enhances the Antibacterial Effect of Methylene Blue-based Photodynamic Therapy on Biofilm-forming Bacteria. *Photochem. Photobiol.* **2019**, *95*, 833–838. [CrossRef]
62. Garcez, A.S.; Núñez, S.C.; Baptista, M.S.; Daghastanli, N.A.; Itri, R.; Hamblin, M.R.; Ribeiro, M.S. Antimicrobial mechanisms behind photodynamic effect in the presence of hydrogen peroxide. *Photochem. Photobiol. Sci.* **2011**, *10*, 483–490. [CrossRef]
63. McCullagh, C.; Robertson, P.K. Photo-dynamic biocidal action of methylene blue and hydrogen peroxide on the cyanobacterium Synechococcus leopoliensis under visible light irradiation. *J. Photochem. Photobiol. B Biol.* **2006**, *83*, 63–68. [CrossRef] [PubMed]
64. Funk, R.S.; Krise, J.P. Exposure of cells to hydrogen peroxide can increase the intracellular accumulation of drugs. *Mol. Pharm.* **2007**, *4*, 154–159. [CrossRef]
65. Huang, Y.-Y.; Choi, H.; Kushida, Y.; Bhayana, B.; Wang, Y.; Hamblin, M.R. Broad-spectrum antimicrobial effects of photocatalysis using titanium dioxide nanoparticles are strongly potentiated by addition of potassium iodide. *Antimicrob. Agents Chemother.* **2016**, *60*, 5445–5453. [CrossRef]
66. Wen, X.; Zhang, X.; Szewczyk, G.; El-Hussein, A.; Huang, Y.-Y.; Sarna, T.; Hamblin, M.R. Potassium iodide potentiates antimicrobial photodynamic inactivation mediated by rose bengal in in vitro and in vivo studies. *Antimicrob. Agents Chemother.* **2017**, *61*, e00467-17. [CrossRef]
67. Huang, L.; Szewczyk, G.; Sarna, T.; Hamblin, M.R. Potassium iodide potentiates broad-spectrum antimicrobial photodynamic inactivation using Photofrin. *ACS Infect. Dis.* **2017**, *3*, 320–328. [CrossRef] [PubMed]
68. Huang, L.; El-Hussein, A.; Xuan, W.; Hamblin, M.R. Potentiation by potassium iodide reveals that the anionic porphyrin TPPS4 is a surprisingly effective photosensitizer for antimicrobial photodynamic inactivation. *J. Photochem. Photobiol. B Biol.* **2018**, *178*, 277–286. [CrossRef] [PubMed]
69. Pinto, S.M.; Henriques, C.A.; Tome, V.A.; Vinagreiro, C.S.; Calvete, M.J.; Dąbrowski, J.M.; Pineiro, M.; Arnaut, L.G.; Pereira, M.M. Synthesis of meso-substituted porphyrins using sustainable chemical processes. *J. Porphyr. Phthalocyanines* **2016**, *20*, 45–60. [CrossRef]
70. Johnstone, R.A.; Nunes, M.L.P.; Pereira, M.M.; Gonsalves, A.M.d.A.R.; Serra, A.C. Improved syntheses of 5, 10, 15, 20-tetrakisaryl-and tetrakisalkylporphyrins. *Heterocycles* **1996**, *7*, 1423–1437.